Experimental and numerical study on the mitigation of autogenous shrinkage of cementitious material

Lu, Tianshi; Liang, Xuhui; Liu, Chen; Chen, Yun; Li, Zhenming

DOI
10.1016/j.cemconcomp.2023.105147

Publication date
2023

Document Version
Final published version

Published in
Cement and Concrete Composites

Cement and Concrete Composites 141 (2023) 105147

Contents lists available at ScienceDirect

Cement and Concrete Composites

journal homepage: www.elsevier.com/locate/cemconcomp

Experimental and numerical study on the mitigation of autogenous shrinkage of cementitious material

Tianshi Lu [a,b], Xuhui Liang [b], Chen Liu [b], Yun Chen [b,c], Zhenming Li [d,*]

[a] School of Civil Engineering and Geomatics, Southwest Petroleum University, Chengdu, China
[b] Department of Materials, Mechanics, Management & Design, Faculty of Civil Engineering and Geoscience, Delft University of Technology, Delft, The Netherlands
[c] School of Materials Science and Engineering, South China University of Technology, Guangzhou, China
[d] Department of Materials Science and Engineering, The University of Sheffield, Sheffield, United Kingdom

ARTICLE INFO

Keywords:
Cement paste
Autogenous shrinkage
Water-repelling agent
Surfactant
Simulation

ABSTRACT

This study experimentally investigated the effects of surfactants and water-repelling agents on the hydration process, relative humidity, and mechanical properties of Portland cement pastes. Based on the measurement results, the degree of hydration, degree of saturation, capillary tension of autogenous shrinkage, and magnitude of autogenous shrinkage were simulated using a numerical model. In the numerical model, the elastic and creep components of autogenous shrinkage were calculated separately, and the creep component was simulated based on the solidification theory. The simulation results indicated that adding admixtures led to lower degrees of hydration and saturation. The capillary tension of the pure Portland cement was larger than that of the other mixtures. This can be attributed to several factors, including the smaller surface tension of mixtures with surfactants, larger contact angle of mixtures with water-repelling agents, and a lower degree of hydration of mixtures with both admixtures. Analyses of the simulated and measured results for different mixtures also show that creep plays an indispensable role in autogenous shrinkage. Adding a surfactant and a water-repelling agent can effectively mitigate autogenous shrinkage. However, when an excessive amount of water-repelling agent was added, its influence on the mitigation of autogenous shrinkage was insignificant.

1. Introduction

Concrete is a brittle material that cracks easily under tension. Cracks are usually found in infrastructures, such as buildings, bridges, highways, and airports. Cracks affect the mechanical performance and accelerate the degradation of cementitious materials and are therefore harmful to the safety, durability, and aesthetics of concrete structures. According to the literature [1–5], restrained shrinkage is a principal reason for cracking. The restraint can be internal (e.g., reinforcement rebar and aggregate [6,7]) or external (e.g., adjacent structures). The mitigation of shrinkage is effective for lowering the risk of cracking and prolonging the service life of concrete structures.

Different types of shrinkage in cementitious systems can be classified based on their mechanisms [8]. For example, chemical shrinkage is the absolute volume reduction during the hydration process, and carbonation shrinkage is caused by the reaction between carbon dioxide and hydrated cement paste in the presence of moisture [9–12]. Among these different types of shrinkage, autogenous shrinkage, which is caused by self-desiccation during the hydration process, has garnered increasing attention due to the widespread use of high-performance concrete with low water-binder ratios [13–18]. Although there is no consensus on the mechanism of autogenous shrinkage, researchers generally agree that a relationship exists between internal relative humidity (RH) and autogenous shrinkage [19,20]. Many studies have shown that reducing the drop in relative humidity can effectively alleviate the autogenous shrinkage of early age cement pastes [21–23].

Over the past decades, numerous methods have been proposed to mitigate autogenous shrinkage, including internal curing and the addition of inert inclusions or expansive agents [24–26]. In addition to these commonly used approaches, the addition of admixtures can effectively mitigate autogenous shrinkage [27]. The mechanisms underlying the effects of different admixtures on autogenous shrinkage are diverse. Surfactants, also known as shrinkage-reducing agents (SRAs), consist of hydrophilic and hydrophobic components [28]. They can decrease the surface tension of the pore solution of the cement paste and consequently reduce autogenous shrinkage [29]. Surfactants exist as

* Corresponding author.
E-mail address: Zhenming.li@sheffield.ac.uk (Z. Li).

https://doi.org/10.1016/j.cemconcomp.2023.105147
Received 26 April 2022; Received in revised form 16 May 2023; Accepted 18 May 2023
Available online 25 May 2023

dispersants, emulsifiers, or detergents [30]. Another commonly used admixture to reduce the autogenous shrinkage of cement paste is a water-repelling agent [31]. By adding a water-repelling agent, the wetting behaviour of the pore wall of cementitious materials and the contact angle between water and the pore wall change [32]. The variation in the contact angle significantly affects the internal force related to self-desiccation, for example, capillary tension [33].

Recently, considerable research has been conducted on the autogenous shrinkage of mixtures with admixtures [33–37]. These studies experimentally investigated the influences of different admixtures on the surface tension, relative humidity, and wetting of cement paste. However, most existing knowledge based on experimental data is qualitative and phenomenological. It is well known that cement paste is a viscoelastic material [38,39], and its deformation includes an instantaneous elastic part and a time-dependent part known as creep [40]. Both the internal driving force and mechanical behaviour, which include the elastic modulus and creep compliance, determine the magnitude of the autogenous shrinkage of cement paste [13,15–17]. These parameters affect the manner in which admixtures mitigate autogenous shrinkage. However, quantitative analyses of the influence of admixtures on these factors are still lacking.

Against this background, a numerical simulation model was used in this study to investigate the effect of the admixture on the internal driving force of autogenous shrinkage and the mechanical behaviour of cement paste. The model calculates the elastic and time-dependent parts of autogenous shrinkage separately, with the latter simulated using the solidification theory and accounting for the changing mechanical properties of the hardening cement paste [41,42]. The investigation focused on Portland cement (CEM I 42.5 N) pastes with and without two admixtures: a nonionic surfactant and a silane emulsion water-repelling agent. The material properties of the cement pastes were experimentally determined and used to simulate the internal driving forces of autogenous shrinkage and hydration. The simulated autogenous shrinkages were subsequently compared with the measured results, and the impact of the admixtures on the mitigation of autogenous shrinkage was analysed.

2. Mechanism of shrinkage mitigating admixtures

Autogenous shrinkage is a macroscopic volume change caused by self-desiccation during the hydration process [19]. While there is a general agreement that autogenous shrinkage is related to changes in the relative humidity caused by self-desiccation, the mechanism of autogenous shrinkage is still under debate [43,44]. The three most frequently discussed mechanisms are the surface tension of solid gel particles, disjoining pressure, and capillary tension [45]. Although the active RH range of the first two mechanisms remains unclear [46,47], capillary tension has recently been widely adopted as the leading mechanism of autogenous shrinkage [48]. This study investigates the shrinkage-mitigating admixtures affected capillary tension and autogenous shrinkage.

According to the Young–Laplace equation [49], the magnitude of capillary tension is calculated as

$$\sigma^{cap} = \frac{2\pi r \bullet \gamma \cos\theta}{\pi r^2} = \frac{2\gamma\cos\theta}{r}, \tag{1}$$

where γ [N/m] is the surface tension of water; θ [−] is the contact angle between the capillary tube wall and air-water interface, and r [m] is the radius of the capillary tube, as shown in Fig. 1.

Cementitious materials are porous mediums [50]. The pore spaces are filled with fluid phases, which are generally air and pore solutions. In addition to the externally applied load, an internal pressure is exerted on the solid skeleton by the fluid phases, which determines the volume change and mechanical performance of the porous medium. The effective stress σ_e depends on the combination of the externally applied load and internal pressure exerted by the fluid phases [51].

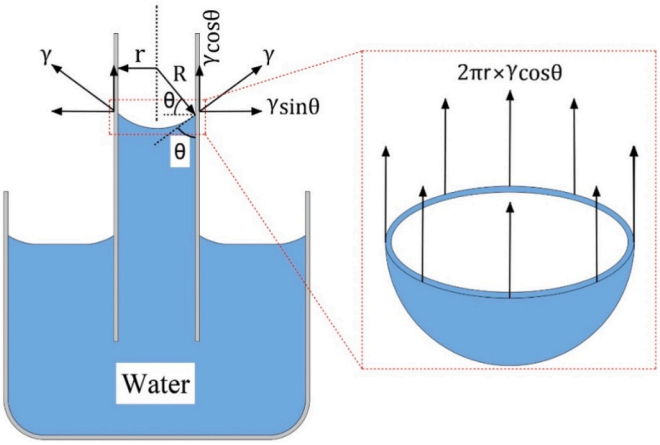

Fig. 1. Schematic representation of the capillary tension.

$$\sigma_e = \sigma + \kappa p^s I, \tag{2}$$

where σ [MPa] is the external applied load tensor; κ [−] is the Biot coefficient [52]; p^s [MPa] is the pressure exerted by the fluid phases on the solid skeleton, and I [−] is the unit second-order tensor.

There is no external applied load σ for the autogenous shrinkage of cement paste. The pressure exerted by the fluid phases on the solid skeleton p^s in Equation (2) can be written as follows [53]:

$$p^s = (1 - S)p^{gas} + Sp^{wat}, \tag{3}$$

where S [−] is the degree of saturation, p^{gas} [MPa] is the gas pressure, and p^{wat} [MPa] is the pressure exerted by water. According to Gawin [53], the gas pressure p^{gas} is negligible compared with the pressure exerted by the water p^{wat}. Capillary tension, disjoining pressure, and surface tension are the three primary constituents of pressure exerted by water. As discussed earlier, the capillary tension σ^{cap} was considered the leading mechanism of autogenous shrinkage in this study, that is, the major component of the pressure exerted by the water p^{wat}. Therefore, $p^{wat} \approx \sigma^{cap}$. Hence, the effective stress, which determines the magnitude of autogenous shrinkage, can be calculated as

$$\sigma_e = \kappa S \sigma^{cap}. \tag{4}$$

According to the Young–Laplace equation (Equation (1)), the surface tension of solution γ, which arises due to the cohesive interactions between molecules in the liquid, is a determining factor of capillary tension. Surfactants are chemical products that include hydrophilic and hydrophobic parts, which can reduce the surface tension, as shown in Fig. 2 [28,54]. When a surfactant is dissolved in water, because the air molecules and the hydrophobic part of the surfactant are nonpolar, the

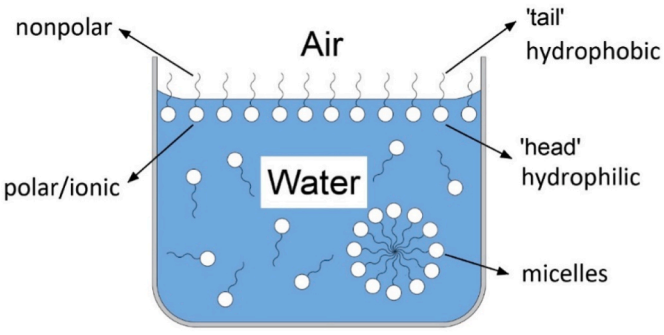

Fig. 2. Schematic representation of the working mechanism of the surfactant (after [54]).

decrease in the dissimilarity of these two contacting phases leads to a reduction in the surface tension of water [28]. Depending on their nature, surfactants can be classified into several different types: anionic, cationic, zwitterionic, and non-ionic [55]. The surfactant (Sika® Control-40) used in this study was nonionic and composed of neopentyl glycol, a double alcohol molecule. More information on Sika® Control-40 can be found in Ref. [36].

Besides the surface tension of water, the contact angle θ between the capillary tube wall and the air-water interface is also a critical factor of capillary tension according to the Young–Laplace equation. Water-repelling agents are chemical admixtures that improve durability and mitigate concrete shrinkage [31,56]. With the addition of a water-repelling agent, the wetting properties of cementitious materials change [57]. The contact angle between the pore solution and the internal pore wall of the concrete increases, which results in a smaller capillary tension, that is, the internal driving force of autogenous shrinkage. The most commonly used water-repelling agents are silanes, siloxanes, and saturated fatty acids [31]. The water-repelling agent used in this study (SILRES ® BS 1802) was a silane emulsion.

3. Materials and experiments

This study used Portland cement (CEM I, 42.5 N) produced by ENCI. Its mean particle size measured with a laser diffraction analyser is 22 μm. The weight ratios of the different mineral components of the Portland cement were 67.1% C_3S, 9.6% C_4AF, 7.8% C_3A, and 5.9% C_2S. The chemical composition of Portland cement is listed in Table 1. Two types of admixtures, a surfactant and a water-repelling agent, were added to the Portland cement paste. The nonionic surfactant (Sika® Control-40), manufactured by SIKA, was composed of neopentyl glycol. The water-repelling/water-repelling agent SILRES® BS 1802 was provided by WACKER. It was a silane emulsion.

Five cement-paste mixtures were investigated in this study. Pure Portland cement paste (CEM I 42.5 N) was used as a reference. Two mixtures were prepared by adding surfactants. The surfactant dosages of these two mixtures were 0.5% and 1.5% by weight of the Portland cement, respectively. Two other mixtures were prepared with the addition of a water-repelling agent. The water-repelling agent dosages of the two mixtures were 0.5% and 1.0% by weight of Portland cement. The water/cement ratio of all mixtures was 0.3. Portland cement and water were mixed in a 5 L epicyclic Hobart mixer. The total mixing time was approximately 3 min [58]. The compositions of all the mixtures are listed in Table 2. In Table 2, the pure Portland cement paste is referred to as in Ref. The two mixtures with the added surfactant were named Surf 0.5 and Surf 1.5, respectively. The other two mixtures, which are added with a water-repelling agent, were named Hydro 0.5 and Hydro 1.0, respectively.

3.1. Hydration heat

The heat flow and cumulative heat generated by the cement paste were measured using a TAM-Air-314 isothermal calorimeter, according to EN 196-8 [59]. Before the test, the machine was calibrated to 20 °C. The calibration lasted for seven days. About 6 g of freshly mixed cement paste was cast into a capped glass vial, and the vial was put in the isothermal calorimeter with a constant temperature of 20 °C. The internal radius of each glass vial was 9 mm. The measurement lasted for seven days, and the measured results were recorded every minute.

Table 1
Chemical composition of Portland cement (% by weight).

CaO	SiO_2	Al_2O_3	Fe_2O_3	SO_3	MgO	K_2O	Na_2O
64.4	20.36	4.96	3.17	2.57	2.09	0.64	0.14

Table 2
Mixture proportions of different kinds of cement paste (water-cement ratio: 0.3).

Name	CEM I 42.5 N (g)	Water (g)	Surfactant (g)	Water-repelling agent (g)
Ref	1000	300	0	0
Surf 0.5	1000	300	5	0
Surf 1.5	1000	300	15	0
Hydro 0.5	1000	300	0	5
Hydro 1.0	1000	300	0	10

3.2. Setting time

According to standard EN 196-3 [60], the initial and final setting times were measured by the Vicat method. The initial setting time is when the penetrating needle is (6 ± 3) mm higher than the base plate. The final setting time was when the steel needle first penetrated only 0.5 mm into the sample.

3.3. Compressive strength

The compressive strength of the cement paste was measured using a servo-hydraulic-controlled testing machine. The specimen was cubic with a size of 40 × 40 × 40 mm^3 and cured under the sealed condition of 20 °C after casting. At curing ages of one, three, and seven days, compressive loading was applied to the specimen using the testing machine until failure. Three replicates were used for each experiment.

3.4. Elastic modulus

The elastic modulus of the cement pastes was continuously measured using a non-destructive test equipment, EMM-ARM [61]. The freshly mixed cement paste was cast into an acrylic tube of length 450 mm. The diameter of the cement paste samples was 16 mm. The tube was then sealed. One end of the tube was fixed to a steel frame, and an accelerometer was placed at the other end. The structural behaviour of the fixed tube is a horizontal composite cantilever, as shown in Fig. 3. The first resonant frequency of the composite cantilever was measured using an accelerometer. The evolution of the elastic modulus was obtained based on the change in the measured frequency. Further details of this test method can be found in Ref. [62]. Three specimens were tested simultaneously for each mixture. The elastic modulus of the specimen was automatically measured every 10 min, and the test duration was seven days.

3.5. Surface tension

The surface tension of the cement paste pore solutions was measured

Fig. 3. Equipment for elastic modulus measurement.

using a Krüss Processor Tensiometer K100 [63]. Deionised water with a surfactant (Sika® Control-40) was used instead of the pore solution extracted from the cement paste. This is because, even though there are different ions in the pore solution, for example, Na^+, K^+, and CL^-, the influence of these ions on the surface tension is much smaller than that of nonionic surfactants [64]. Approximately 35 ml of water with the surfactant was poured into a glass vessel with a capacity of 121.5 ml. The glass vessel was then placed under a Krüss standard plate (Fig. 4a) connected to a Krüss Processor Tensiometer K100 (Fig. 4b). The Krüss standard plate measured 19 mm × 10 mm × 0.2 mm. The plate was then immersed in the solution and pulled off. The Krüss Processor Tensiometer K100 recorded the force required to pull the plate out of the water, which can be used to obtain the surface tension. Ten measurements were performed within 1 min. The average value of the 10 performances was considered as the surface tension.

3.6. Hydrophilicity

Approximately 15 g of the cement paste was cast and cured under sealed conditions. At the ages of 3 and 7 d, a drop of water (0.05 ml) was placed on the surface of the specimen using a burette. Images of the drops in contact with the surface, which were used to analyse the hydrophilicity of the mixtures, were captured using a camera 10 s after the droplet was placed.

3.7. Internal relative humidity

The internal relative humidity was measured using HC2-AW measuring cells which were connected to a Rotronic hygroscopic DT station. The freshly mixed cement paste was cast into a sample with a diameter of 30 mm and a thickness of 7 mm. The samples were placed in a steel chamber. Subsequently, the chamber was covered with HC2-AW measuring cells and placed in the thermostatic water bath at 20 °C. The two samples were tested simultaneously, and the difference between the two measurements was less than 0.5%. The measurement was started one day after casting to avoid the moisture compensation of the cells. The internal relative humidity of the samples was measured every 2 min, and the measurement lasted till seven days after casting.

3.8. Autogenous shrinkage

This study measured the change in the length of the specimen in the corrugated tube to determine the autogenous shrinkage of the cement paste according to ASTM C1698-09 [65]. The tube was made of low-density polyethylene. The length and diameter of the tubes were 430 mm and 29 mm, respectively. After the mixing, the cement paste was cast into a tube and sealed with plastic plugs. The specimens were then placed on metal shelves. The tube length was automatically measured by linear variable differential transformers every 10 min, and the test lasted for seven days. Three replicates were tested simultaneously for each mixture.

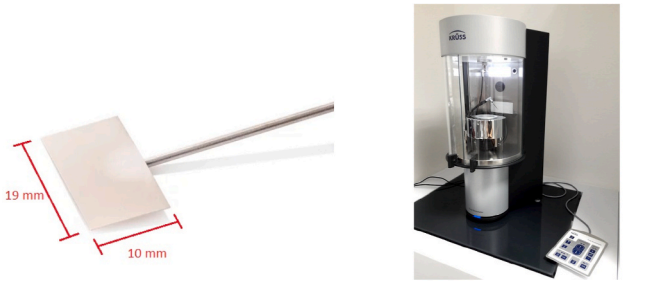

(a) Krüss standard plate (b) Krüss Processor Tensiometer K100

Fig. 4. Apparatus for surface tension measurement.

4. Experimental results and discussion

4.1. Hydration heat

The measured heat flow and cumulative heat of all mixtures are presented in Fig. 5a and b, respectively. During the hydration process, several complex chemical reactions occur, and hydration heat is liberated. According to Lehmann [50], a linear relationship exists between the degree of hydration and liberated heat. The hydration heat can be used to indicate the hydration rate [66].

As shown in Fig. 5a, there is an initial peak caused by the dissolution of the cementitious material into the water, followed by a dormant period. After the dormancy period, the heat flow accelerated and reached two sequential peaks. According to Mindess et al. [67], these two peaks were caused by the hydration of tricalcium silicate and tricalcium aluminate, respectively. During this period, the hydration rate of the cementitious material is high. Fig. 5a shows two peaks for all mixtures. However, the magnitudes of the two peaks differed in the mixtures. The two measured peaks of the mixtures with the addition of surfactants (Surf 0.5 and Surf 1.5) are lower than that of Portland cement paste. This result is consistent with the findings of Zuo et al. [67,68]. According to Zuo et al. [67], this is because the addition of surfactant retards the hydration process and then lowers the height of the heat flow. After these two peaks, the hydration rate gradually decreased because the continuously formed hydration products surrounded the unhydrated cement particles and inhibited their further dissolution [50].

From the comparison between the measured cumulative heat of different mixtures (Fig. 5b), it can be observed that the mixtures with the addition of a surfactant or water-repelling agent released less heat than the pure Portland cement paste during the first seven days. This is consistent with the findings of Qu et al. [33] and Feiji [36]. As shown in Fig. 2, when a surfactant is dissolved in water, a layer of surfactant molecules covers the surface of the water, preventing contact between the water and cement particles. Less cement dissolves in water, resulting in a lower hydration rate and less heat release [28]. Qu et al. [33] reported a similar water-repelling mechanism.

4.2. Setting time

Fig. 6 shows the measured initial and final setting times for different mixtures. Setting is a process caused by hydration reactions and results in the gradual development of the rigidity of a cementitious mixture [69]. The initial and final settings were related to the continuous hydration of the cement [70]. Fig. 6b shows that the final setting times of mixtures with the addition of the water-repelling agent (Hydro 0.5 and Hydro 1.0) are shorter than that of Portland cement paste. Lu et al. [71] observed that the bleeding phenomenon was found in fresh mixtures with the addition of a water-repellent admixture during the first few hours of mixing. Bleeding leads to a denser solid phase of the cement paste during the dormant period and a shorter final setting time of Hydro 0.5 and Hydro 1.0 [72].

4.3. Compressive strength

The measured compressive strengths as functions of the ages of the different mixtures are shown in Fig. 7. The compressive strength of the samples with the water-repelling agent was lower than that of the reference during the first seven days. The higher the dosage of the water-repelling agent, the lower the measured compressive strength of the sample. This experimental result is consistent with those reported by Liu et al. [73] and Shahbazi et al. [74]. According to Henk [75], an increase in strength is related to the evolution of the microstructure of the cement paste during the hydration process. As discussed in Section 4.1, the hydration rate of the mixtures with the addition of a water-repelling agent was lower than that of Portland cement paste during the first

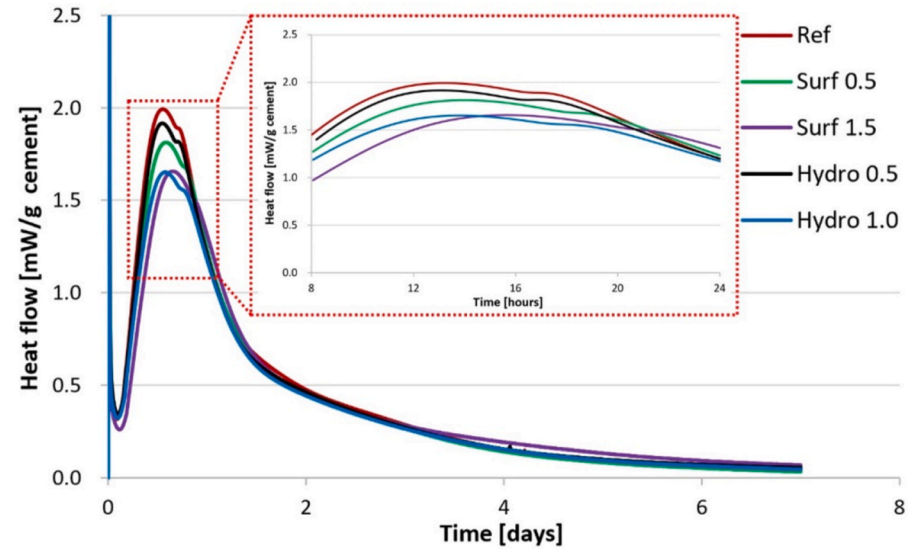

(a) Heat flow

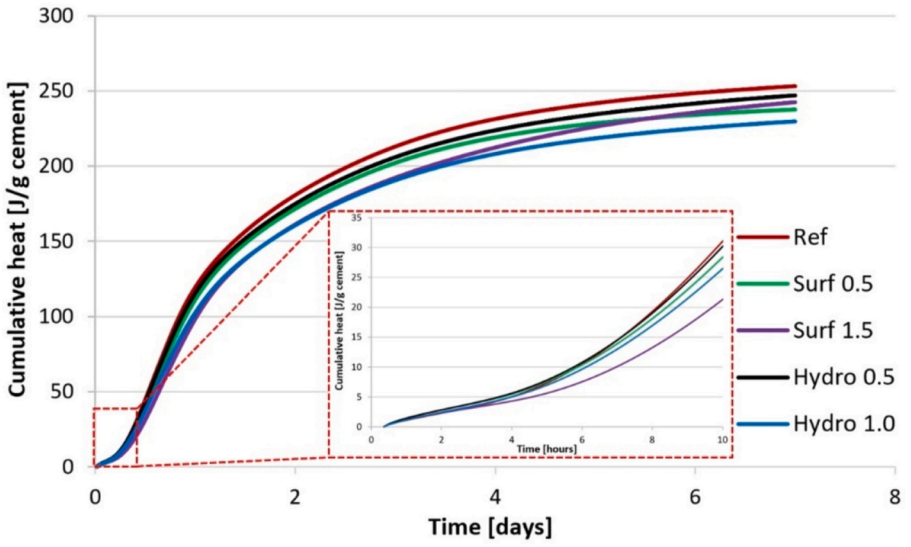

(b) Cumulative heat

Fig. 5. Measured heat flow and cumulative heat by the cement mass with time.

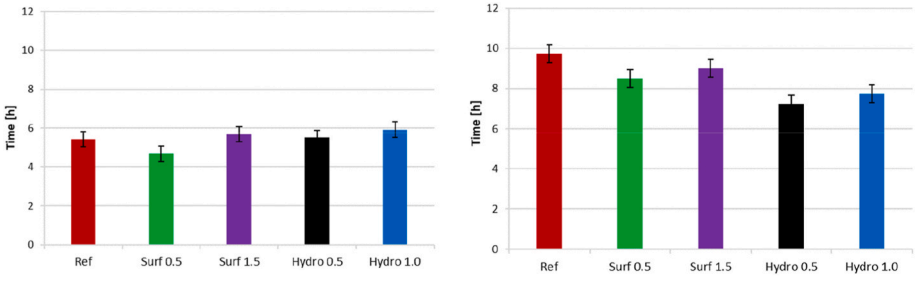

(a) Initial setting time (b) Final setting time

Fig. 6. Measured setting time of different mixtures.

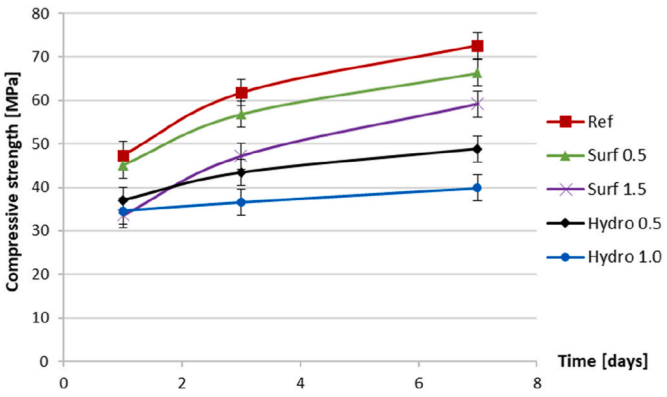

Fig. 7. Measured compressive strength of different mixtures.

seven days. A lower degree of hydration led to a looser skeleton structure and lower compressive strength. The same reason can also be applied to the cases of Surf 0.5 (green line) and Surf 1.5 (purple line). Apart from the degree of hydration, other factors influencing the compressive strength of the samples with a water-repelling agent were bleeding and reabsorption. As explained in Section 4.2, for mixtures containing a water-repelling agent, bleeding occurs during the dormant period, leaving a layer of water over the surface. At a later age, the water layer was reabsorbed into the cement paste, leading to a lower compressive strength [72]. Bleeding and reabsorption resulted in a lower compressive strength of mixtures with the addition of a water-repelling agent compared with that of mixtures with the addition of a surfactant with a similar degree of hydration.

4.4. Elastic modulus

The measured elastic moduli of the five cement-paste mixtures are shown in Fig. 8. The elastic modulus of the mixtures decreased with the increase in the surfactant dosage. This phenomenon has also been reported previously [76]. Similar to the compressive strength, the looser skeleton structure of cement pastes with surfactants, which is related to the lower degree of hydration, is the primary reason for the decrease in the elastic modulus. Fig. 8 also shows that adding a water-repelling agent has a negative effect on the development of the elastic modulus; however, the dosage was not a crucial factor. The elastic modulus of Hydro 1.0 (blue line) is similar to that of Hydro 0.5 (black line) after two days, even when the compressive strength of Hydro 1.0 is much lower than that of Hydro 0.5. In addition to strength, another crucial factor influencing the elastic modulus is the water content of the specimen [77]. The elastic modulus of concrete increased with the water content; that is, the value of the elastic modulus of the wet specimen was higher

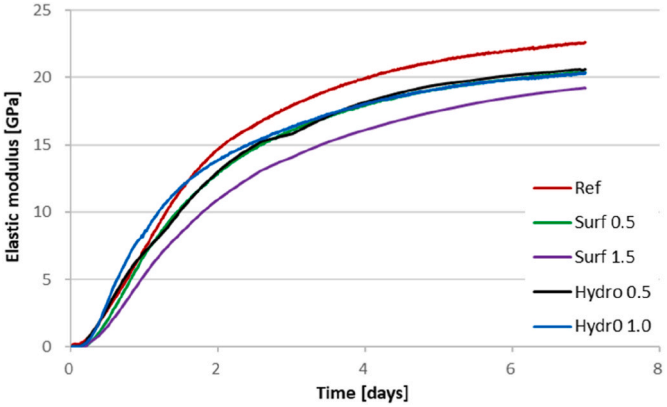

Fig. 8. Measured elastic modulus of different mixtures.

than that of the dry specimen with the same strength. According to Liu et al. [78], this can be attributed to the free water in the internal pores, which relieves the softening effect caused by empty pores and microcracks during deformation [79]. From Fig. 15 in Section 5.2, it will be confirmed that the degree of saturation of Hydro 1.0 (blue line) is higher than that of Hydro 0.5 (black line). More water contents in Hydro 1.0 can be why the elastic modulus of Hydro 1.0 (blue line) is similar to that of Hydro 0.5 (black line) at seven days, even when the compressive strength of Hydro 1.0 is much lower than that of Hydro 0.5.

4.5. Surface tension

The measured surface tension of water in the presence of the surfactant is shown in Fig. 9a. To study the relationship between the surface tension and surfactant dosage, a synthetic pore solution of cement paste with surfactant/cement weight ratios of 0, 0.5%, 1.5%, and 2.5% was tested. The measured surface tension of reference (Ref) is 0.0726 N/m; this is according to the value reported by Vargaftik et al. [80]. Fig. 9a also shows that the surface tension of the pore solution decreases with the addition of the surfactant. As explained in Section 2, a layer of the hydrophobic surfactant molecules covers the surface of the water. A decrease in the dissimilarity between the contacting air molecules and the hydrophobic part of the surfactant reduces the surface tension of water. It should also be noted that the decrease in surface tension was not linear with surfactant dosage (Fig. 9b). When the surfactant/cement weight ratio increased from 0 (Ref) to 0.5% (Surf 0.5), the surface tension of the pore solution decreased from 0.0726 to 0.0648 N/m. However, when the surfactant/cement weight ratio increased from 1.5% (Surf 1.5) to 2.5% (Surf 2.5), the surface tension of the pore solution decreased from 0.0555 to 0.0518 N/m. According to Rosen [28], when the surfactant concentration is beyond a certain value, excess surfactant will start to form micelles in the solution instead of covering the surface of the water (Fig. 2), and the effectiveness of the surfactant molecules will decline.

4.6. Hydrophilicity

The images of the water droplets on the surfaces of the reference and mixtures with the water-repelling agent (0.5% and 1.0%) at ages of 3 and 7 d are presented in Fig. 10. As shown in Fig. 10a and d, the water droplet spreads and immediately gets immersed into the reference, which illustrates the hydrophilicity of the Portland cement paste surface.

It can also be noticed from Fig. 10 that the water droplets on the surfaces of mixtures with a water-repelling agent, i.e., Hydro 0.5 and Hydro 1.0, keep a bead shape at three and seven days. The wetted area of the mixed surface decreases. This phenomenon demonstrates that the sample surfaces changed from hydrophilic to hydrophobic by adding the water-repelling agent. The comparison between Fig. 10e and f shows that the contact angle θ between the air-water interface and the sample surface (Equation (1)) of Hydro 0.5 and Hydro 1.0 are similar at seven days. The effect of the water-repelling agent dosage on the wetting properties of the samples was not significant. Qu et al. [33] and Shahbazi et al. [74] reported similar results. This indicates that there is an optimum dosage of the water-repelling agent. Beyond the optimum dosage, the hydrophilicity of the samples did not change significantly with increasing water-repelling agent dosage.

4.7. Internal relative humidity

The measured internal relative humidity of the different mixtures is shown in Fig. 11a. After the start of the measurements, the measured values increased over a short period and then gradually declined. This is because the moisture equilibrium between the sample and sensor was reached during this short period. As shown in Fig. 11a, the maximum measured relative humidity of all the samples was lower than 100%.

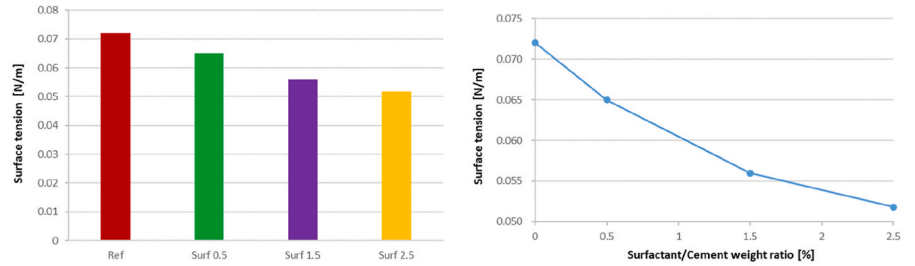

(a) Measured surface tension of pore solutions (b) Relationship between surface tension and surfactant dosage

Fig. 9. Surface tension of different synthetic pore solutions.

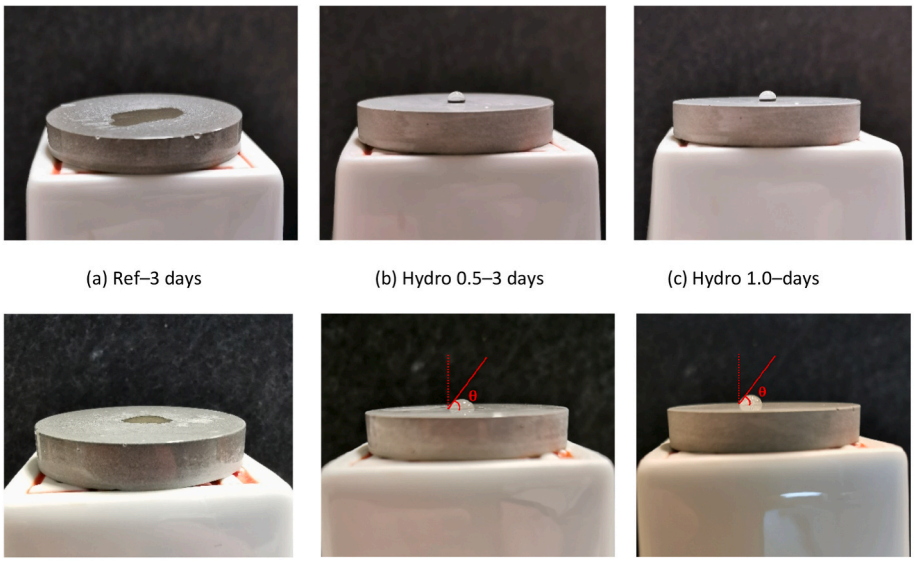

(a) Ref–3 days (b) Hydro 0.5–3 days (c) Hydro 1.0–days

(d) Ref–7 days (e) Hydro 0.5–7 days (f) Hydro 1.0–7 days

Fig. 10. Images of a water droplet on the surface of the mixtures with and without a water-repelling agent at ages of 3 and 7 d.

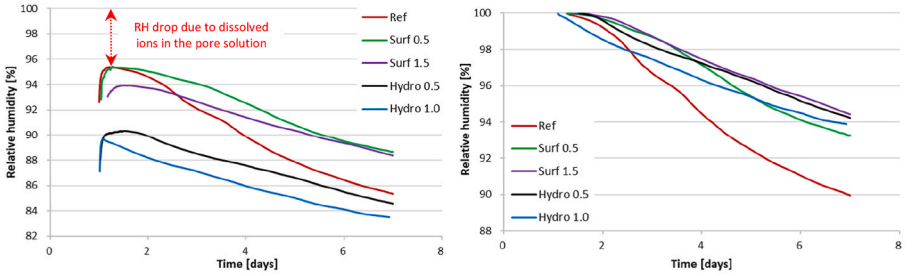

(a) Measured internal relative humidity (b) Relative humidity RH_K related to the air-water menisci

Fig. 11. Measured internal relative humidity *RH* and relative humidity related to air-water menisci RH_K of different mixtures.

This phenomenon has also been previously reported [13,81,82]. The measured internal relative humidity was the result of the combined effects of the air-water menisci and dissolved ions in the pore solution (Equation (5)). The initial drop in the relative humidity can be attributed to the dissolved ions in the pore solution when the sample is still saturated [83]. For different mixtures, the effect of dissolved ions on the initial relative humidity changed with ion concentration. This study assumed that the initial drop in relative humidity is caused only by dissolved ions, and the effect remains constant [13]. By removing the effect of the dissolved ions, the evolution of the relative humidity related to the change in the air-water menisci is shown in Fig. 11b.

Fig. 11b shows that the drops in the relative humidity of the mixtures with the addition of the surfactant and water-repelling agent are smaller than those of the reference. This is consistent with the findings of Bentz et al. [84]. The higher relative humidity of the mixtures containing the surfactant and water-repelling agent at 7 d can be attributed to two reasons. According to Kelvin's equation, the internal relative humidity is related to the surface tension and contact angle between the capillary tube wall and air-water interface, which can be expressed as [85].

$$ln\ RH_K = ln\frac{RH}{RH_S} = \frac{-2\gamma V_m}{R_u TR} = \frac{-2\gamma V_m\ cos\ \theta}{R_u Tr}, \quad (5)$$

where RH_K [−] is the internal relative humidity related to air-water

menisci; RH [−] is the measured relative humidity; RH_S is the effect of the dissolved ions on relative humidity; γ [N/m] is the surface tension of the pore solution; V_m [m^3/mol] is the molar volume of the pore solution; R_u [J/(mol • K)] is the universal gas constant; T [K] is the absolute temperature; θ [−] is the contact angle between capillary tube wall and air-pore solution interface; r [m] is the radius of the capillary tube; R [m] is the Kelvin radius, i.e., the radius of the air-water meniscus. The relationship between the radius of the capillary pore r and the Kelvin radius R is $r = R\ cos\ \theta$ (as shown in Fig. 1).

The relative humidity RH_K of the samples with a smaller surface tension or larger contact angle was higher than that of samples with the same radius as the water-filled capillary pore. The smaller surface tension of the samples with the addition of the surfactant (Fig. 9a) and the larger contact angle of the samples with the addition of the water-repelling agent (Fig. 10) partly lead to a higher relative humidity RH_K.

However, the degree of hydration of the samples with the addition of surfactant and water-repelling agent was less than that of the reference, as indicated by the cumulative heat (Fig. 5b). A lower degree of hydration (Fig. 14a) resulted in more free water in the pore structure and, thus, a higher degree of saturation (Fig. 15) and relative humidity. This result is confirmed by the numerical simulation described in Section 5.2.

4.8. Autogenous shrinkage

Fig. 12 shows the measured deformation as a function of the age of the different cement pastes. After mixing, the cement paste was cast into a tube, and the change in the length of the samples was measured.

Fig. 12 shows that the deformation of the cement pastes after mixing can be divided into several distinct stages. During the first several hours after mixing, shrinkage develops rapidly, followed by a short stage of swelling. Over the past few decades, several mechanisms have been proposed to explain early age swelling. Examples include crystal pressure and ettringite formation [86,87]. Due to the addition of water-repelling agents, the water absorption of cement paste due to bleeding is also a significant reason for the early age swelling for Hydro 0.5 and Hydro 1.5 [88]. The samples shrank steadily after this swelling stage. The magnitude of the deformation at different stages differs significantly, and no single mechanism can explain the entire process of deformation. Part of the deformation that should be considered autogenous shrinkage is still debatable in the scientific community. The Japan Concrete Institute (JCI) [19] measures autogenous shrinkage after the initial setting time, whereas the final setting time is considered as the beginning of autogenous shrinkage in the American Standard Test Method (ASTM) [65]. Miao et al. [89] proposed that setting is a physical manifestation of progressive hydration, but the measured values are arbitrary [90]. The beginning of autogenous shrinkage should be related to the setting time but not necessarily identical. Miao et al. [89] used meniscus depression measurement to determine the "time-zero" of autogenous shrinkage, but further comprehensive investigations are still required to scientifically determine the "time-zero" of autogenous shrinkage using this method [37]. Bjøntegaard [91] proposed that the time when maximum (macroscopic) swelling is observed can be considered as the starting time of autogenous shrinkage. This is because the samples shrink steadily after the short-time swelling, and the relationship between the development of shrinkage and the drop of the internal relative humidity is explicit during this period. This study considered the shrinkage after the maximum swelling to be the autogenous shrinkage of the cement pastes, as shown in Fig. 13. It can be observed that the addition of admixtures has a significant effect on the autogenous shrinkage. The effect of admixtures on the autogenous shrinkage is discussed in Section 5.4.

5. Simulation of material parameters and autogenous shrinkage

As explained in Section 2, to calculate the effective stress, which determines the magnitude of autogenous shrinkage, several material parameters must be determined first, namely, the degree of hydration α, degree of saturation S, and capillary tension σ^{cap}.

5.1. Degree of hydration

The degree of hydration α [−] is defined as the fraction of reacted cement relative to the amount of cement [50]. It can be indicated with the heat of hydration as [92]:

$$\alpha(t) = \frac{Q(t)}{Q_{max}}, \tag{6}$$

where $Q(t)$ [J/g] is the cumulative heat of hydration liberated at time t, and Q_{max} [J/g] is the maximum amount of heat liberated at complete hydration. According to van Breugel [50], the maximum hydration heat of Portland cement Q_{max} can be calculated as the sum of the maximum hydration heat of different mineral components. The weight ratios of the mineral components of the cement used in this study (CEM I 42.5 N) are presented in Section 3. The maximum amount of hydration heat for different mineral components can be found in the literature [93]. The calculated maximum hydration heat is 525 J/g. Similar results were reported in other references [50,94].

The calculated degrees of hydration of different mixtures based on the measured cumulative heat of hydration (Fig. 5b) are shown in Fig. 14a.

Ye [94] reported similar results for Pure Portland cement paste (Fig. 14c). According to Ye, the degree of hydration of pure Portland cement paste with a water-cement ratio of 0.3 is approximately 50% at 168 h (Fig. 14c). The calculated degree of hydration of (CEM I 42.5 N cement paste with a water-cement ratio of 0.3), which was calculated using Equation (6), is also approximately 50%, as shown in Fig. 14b. As

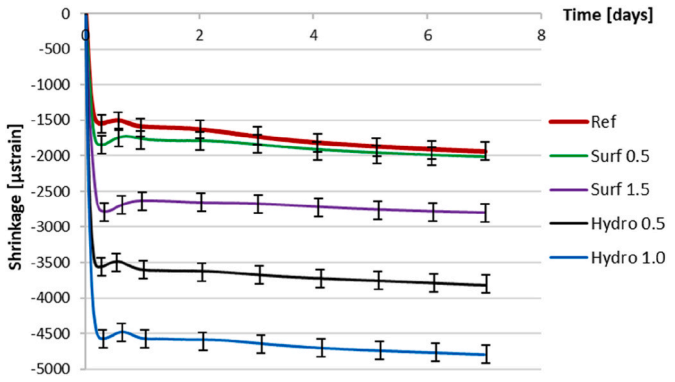

Fig. 12. Measured deformation of different mixtures (starting time: after mixing).

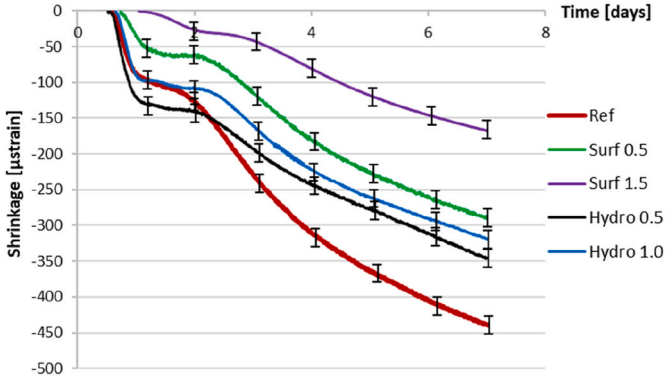

Fig. 13. Measured deformation of different mixtures (starting time: after maximum swelling).

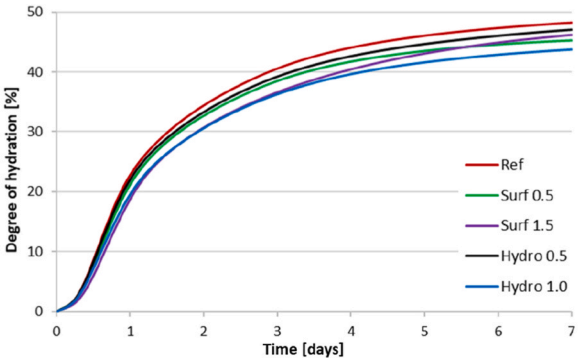

(a) Degree of hydration calculated using Equation 6

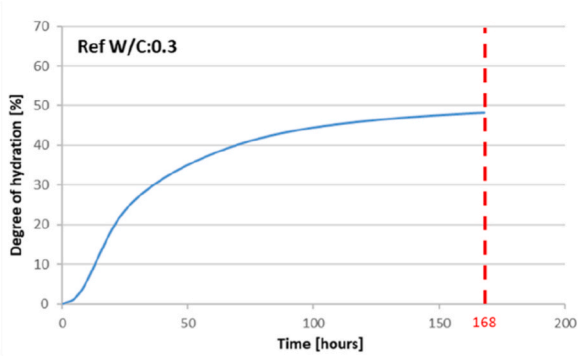

(b) Degree of hydration of Ref. calculated using Equation 6

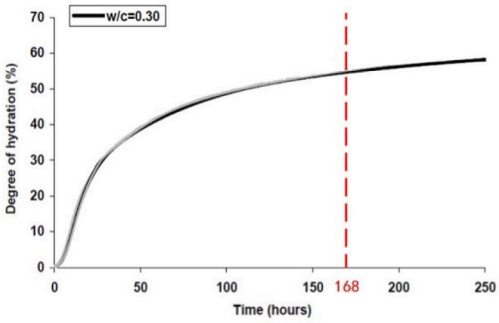

(c) Degree of hydration calculated by Ye

Fig. 14. Calculated degree of hydration of different mixtures.

shown in Fig. 14a, the degree of hydration of the mixtures with the addition of a surfactant or water-repelling agent was lower than that of pure Portland cement paste during the first seven days.

5.2. Degree of saturation

According to Powers [95], the degree of saturation S [−] can be determined as the ratio of the evaporable water content V_{ew} [m^3/m^3] to the pore volume of the cement paste V_p [m^3/m^3] as

$$S = \frac{V_{ew}}{V_p} = \frac{V_{cw} + V_{gw}}{V_{cw} + V_{gw} + V_{cs}}, \tag{7}$$

where V_{cw} [m^3/m^3] is capillary water, V_{gw} [m^3/m^3] is gel water, and V_{cs} [m^3/m^3] is chemical shrinkage.

For Portland cement paste (CEM I 42.5 N) used in this study, Jensen and Hansen [96,97] proposed the expressions of capillary water, gel water, and chemical shrinkage as functions of the degree of hydration of cement paste α. Then Equation (7) can be written as

$$S = \frac{P - 0.72(1-P)\alpha}{P - 0.52(1-P)\alpha}, \tag{8}$$

where P [−] is the initial porosity of the cement paste. The volume ratio between the water and cement paste can be calculated as follows:

$$P = \frac{w/c}{w/c + \rho_w/\rho_c}, \tag{9}$$

where w/c is the water-cement ratio; ρ_w [kg/m^3] is the density of water, and ρ_c [kg/m^3] is the density of cement, whose value is taken as 3150 kg/m^3 [98].

The degree of saturation of the various mixtures was calculated using Equation (8) based on the previously calculated degree of hydration (Fig. 14a).

The calculated results are presented in Fig. 15. Similar results can be found in the literature [13,16]. Fig. 15 shows that the degree of saturation of the mixtures increased with adding a surfactant or water-repelling agent. As explained in Section 5.1, less cement dissolved and reacted with water for the mixture with admixtures during the first seven days. Fewer water molecules are consumed during the hydration reaction. More free water exists in the pore structures, leading to a higher degree of saturation.

5.3. Capillary tension

As mentioned in Section 2, the capillary tension can be calculated

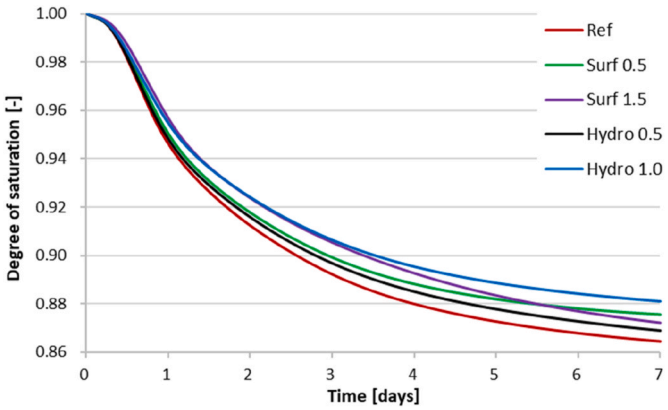

Fig. 15. Calculated degree of saturation of different mixtures.

using the Young–Laplace equation which is a function of the radius of the largest water-filled capillary pore (Fig. 1). According to Kelvin's equation (Equation (5)), there is a relationship between relative humidity and the radius of the largest water-filled capillary pore. By substituting Equation (5) into Equation (1), the capillary tension can be calculated as follows:

$$\sigma^{cap} = \frac{-R_u T \ln \frac{RH}{RH_S}}{V_m} = \frac{-R_u T \ln RH_K}{V_m}. \tag{10}$$

The calculated capillary tension of the different mixtures based on the internal RH (Fig. 11b) using Equation (10) is shown in Fig. 16 as a function of age. These results are in accordance with those reported by Lebental et al. [99]. From Fig. 16, it can be observed that the capillary tension of pure Portland cement was larger than that of the other mixtures. This could be attributed to several factors. First, the surface tension of the mixtures with the addition of the surfactant was smaller than that of the reference, which resulted in a lower RH_K (Equation (5)) and a smaller capillary tension (Equation (10)). Second, the contact angle between the capillary tube wall and the air-water interface of the mixtures with the water-repelling agent was larger than that of the reference (Fig. 10). According to the Young–Laplace equation (Equation (1)), the capillary tension of a sample decreases with an increasing contact angle for samples with the same pore size. Fig. 16 also shows that the capillary tension of Hydro 0.5 and Hydro 1.0 is quite close at seven days. This is consistent with the contact angle measurements (Fig. 10e and f). Third, the lower degree of hydration (Fig. 14a) of the mixtures with admixtures led to more free water in the pore structure and a higher degree of saturation (Fig. 15). The radius of the largest water-filled capillary pore increased, and the capillary tension decreased with the addition of admixtures (Equation (1)).

5.4. Autogenous shrinkage

However, cementitious materials are not ideally elastic. The deformation of cementitious materials is composed of elastic and creep components.

$$\varepsilon(t) = \varepsilon_e(t) + \varepsilon_c(t), \tag{11}$$

where $\varepsilon(t)$ [−] is the total deformation of cementitious materials; $\varepsilon_e(t)$ [−] is the elastic component of deformation, and $\varepsilon_c(t)$ [−] is the creep component of deformation.

According to Hooke's law, the elastic component of deformation can be expressed as

$$\varepsilon_e(t) = \frac{\sigma(t)}{E(t)}(1 - 2\vartheta), \tag{12}$$

where ϑ [−] is the Poisson's ratio; $\sigma(t)$ [MPa] and $E(t)$ [MPa] are the load and the elastic modulus of cementitious materials at time t, respectively.

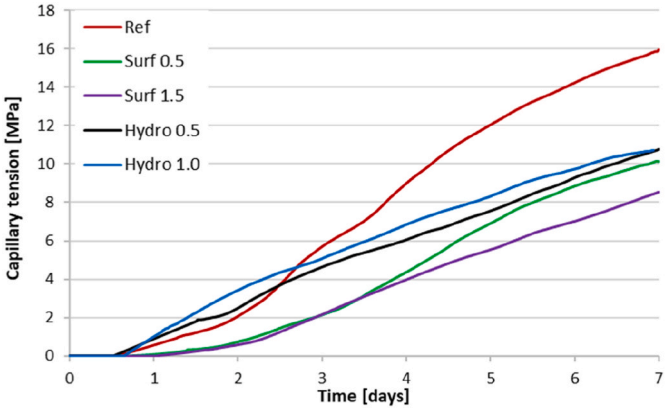

Fig. 16. Calculated capillary tension of different mixtures.

When cementitious materials are subjected to a sustained load, their deformation continues to increase, which is known as creep. Creep and stress relaxation, that is, the loss in stress when cementitious materials are held at a constant strain, are the two forms of viscoelastic behaviour of cementitious materials. It has been reported that pore water and the hydration product, calcium silicate hydrate (CSH), play a critical role in the viscoelastic behaviour [15,39,100]. Recently, numerous numerical models have been proposed to predict creep development [101–106]. This study adopted a numerical simulation model proposed by Hedegaard [52], which is based on solidification theory [107,108], to predict the creep part of autogenous shrinkage. In this model, the creep compliance $J(t, t_0)$ [MPa^{-1}], which describes the development of the time-dependent strain as a function of time, is expressed as follows:

$$J(t,t_0) = \frac{1}{E_i} + \left(\frac{P_1}{K}\right)\left(\frac{1}{t_0 - \beta}\right) ln\left[\frac{t_0}{t}\left(\frac{t - t_0}{\beta} + 1\right)\right] + P_1\, ln\left(\frac{t - t_0}{\beta} + 1\right) + \left(\frac{P_2}{Kt_0}\right)\left(\frac{t - t_0}{t}\right) + P_2\, ln\frac{t}{t_0}, \tag{13}$$

where E_i [MPa] is the instantaneous modulus, which is related to the elastic modulus E [MPa] and taken as 1.43 E in this study [42]; P_1 [MPa^{-1}] is the nonaging viscoelastic compliance constant, related to the compressive strength [52] and expressed as $20.7e^{-0.06f_c}$ in this study; K [$days^{-1}$] is the rate constant whose value is 0.5; t_0 [days] is the time at loading; β [days] is the time constant whose value is 2×10^{-5}; P_2 [MPa^{-1}] is the flow constant taken as 7×10^{-6} [42].

Based on Equation (13), the creep compliance rate at a given time t_n can be written as

$$\dot{J}(t_n, t_0) = \left(\frac{1}{Kt_n} + 1\right)\left(\frac{P_1}{t - t_n + \beta} + \frac{P_2}{t_n}\right). \tag{14}$$

If the time interval Δt is small, the increment of creep $\Delta\varepsilon_c(t_n)$ during the period t_n to time $t_n + \Delta t$ can be calculated as:

$$\Delta\varepsilon_c(t_n) = \sigma(t_n)\dot{J}(t_n, t_0)\Delta t = \sigma(t_n)\left(\frac{1}{Kt_n} + 1\right)\left(\frac{P_1(t_n)}{t_n - t_0 + \beta} + \frac{P_2}{t_n}\right)\Delta t, \tag{15}$$

where $\sigma(t_n)$ is the load at time t_n.

The creep $\varepsilon_c(t_{n+1})$ at time t_{n+1} can be calculated as the summation of the increments of creep that formed at subsequent time intervals before time t_{n+1} and can be expressed as

$$\varepsilon_c(t_{n+1}) = \Delta\varepsilon_c(t_n) + \varepsilon_c(t_n) = \frac{\sigma(t_n)}{E_i(t_n)} + \sigma(t_n)\left(\frac{1}{Kt_n} + 1\right)\left(\frac{P_1(t_n)}{t_n - t_0 + \beta} + \frac{P_2}{t_n}\right)\Delta t + \sum_{i=1}^{n}\Delta\varepsilon_c(t_i)\,. \tag{16}$$

For a cement paste under an internal load, that is capillary tension, which is the case of autogenous shrinkage, combining Equations (4) and (16), the creep part of the autogenous shrinkage can be calculated as follows:

$$\varepsilon_c(t_{n+1}) = \frac{S\sigma^{cap}(t_n)\kappa(1 - 2\vartheta)}{E_i(t_n)} + S\sigma^{cap}(t_n)\kappa(1 - 2\vartheta)\left(\frac{1}{Kt_n} + 1\right)\left(\frac{P_1(t_n)}{t_n - t_0 + \beta} + \frac{P_2}{t_n}\right)\Delta t + \sum_{i=1}^{n}\Delta\varepsilon_c(t_i). \tag{17}$$

This study calculated the total autogenous shrinkage as the sum of the elastic and creep parts. The elastic and creep parts were calculated using Equations (12) and (17) separately. A flowchart of the calculation procedure is presented in Fig. 17.

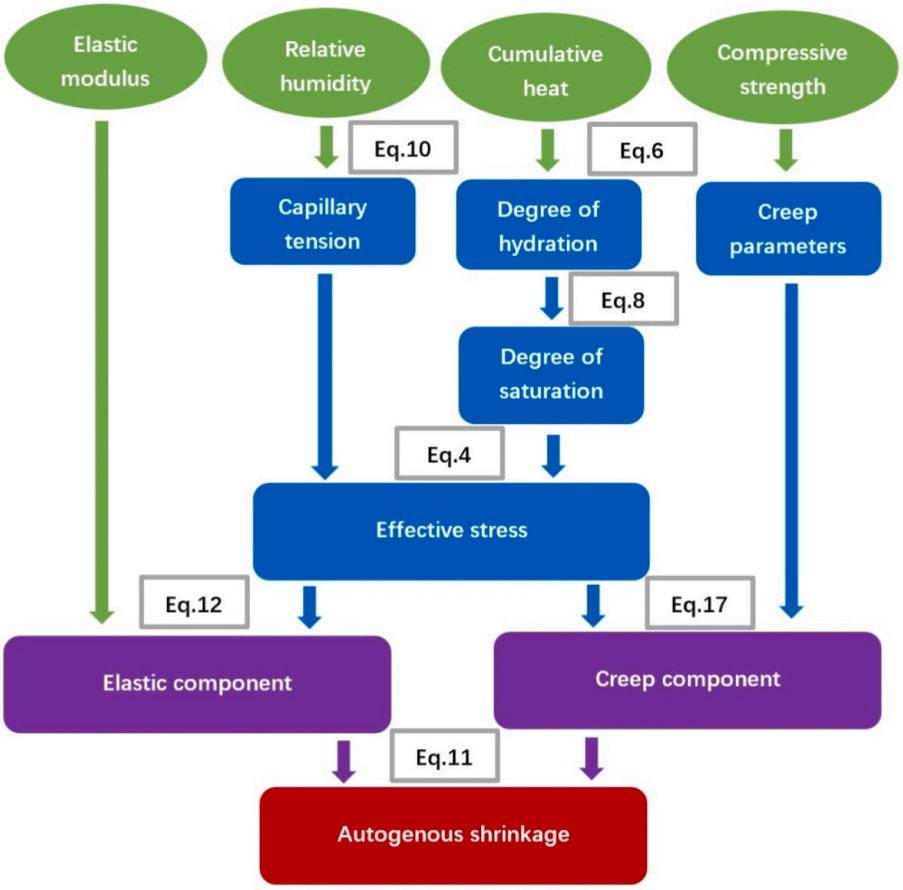

Fig. 17. Flow chart of the simulation model of autogenous shrinkage.

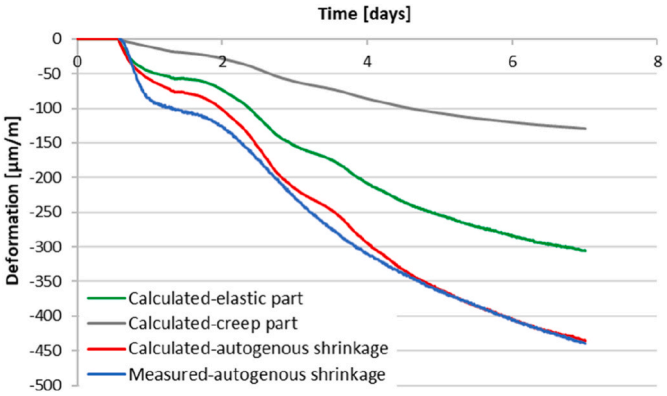

Fig. 18. Measured and calculated autogenous deformation of Portland cement paste after maximum swelling.

5.4.1. *Reference-portland cement paste*

Fig. 18 presents the measured and calculated autogenous deformations of Portland cement paste with a water-binder ratio of 0.3 after the maximum swelling. The contributions of the elastic and creep parts to the autogenous shrinkage are shown separately in this figure. From Fig. 18, it can be observed that the autogenous shrinkage trend of Portland cement paste is predicted using a numerical model, which considers creep. Fig. 18 also shows a significant increase in the deformation rate at the age of two days. According to the calculated results, this was primarily due to an increase in the rate of capillary tension (red line in Fig. 16). The calculation of the autogenous shrinkage of Portland cement paste indicates that there is a close relationship between autogenous shrinkage and changes in the internal relative humidity.

5.4.2. *Portland cement paste with the addition of surfactant*

In Fig. 19a and b, the measured and calculated autogenous shrinkages of Portland cement pastes with the addition of surfactants are shown. The dosages of the surfactant were 0.5% (Surf 0.5) and 1.5% (Surf 1.5) by the weight of Portland cement.

By analysing the measured results of autogenous shrinkage (blue lines in Fig. 19a and b), it can be observed that autogenous shrinkage decreases significantly with increasing surfactant dosage. At the age of seven days, the magnitude of shrinkage decreased from 300 to 160 m/m when the surfactant/water weight ratio of the mixtures increased from 0.5% to 1.5%. As shown in Fig. 16, capillary tension, which is the internal driving force of autogenous shrinkage, decreased markedly with the addition of the surfactant. While the elastic modulus of the mixtures also decreased with increasing surfactant dosage (Fig. 8), the change in the elastic modulus was much smaller than that of the capillary tension. The larger drop in capillary tension plays a dominant role in the decrease in the autogenous shrinkage of the mixture with the addition of Surf 0.5 and Surf 1.5 (Equations (12) and (17)).

5.4.3. *Portland cement paste with addition of water-repelling agent*

The measured and calculated autogenous shrinkages of the Portland cement pastes with the addition of a water repellent are shown in Fig. 20a and b.

As shown in Fig. 20, the autogenous shrinkage of the mixtures decreased with the addition of the water-repelling agent; however, the dosage did not play a crucial role. When the admixture/water weight ratio of the mixtures was increased from 0% to 0.5%, the autogenous shrinkage decreased from 450 m/m (Fig. 18) to 350 m/m (Fig. 20a).

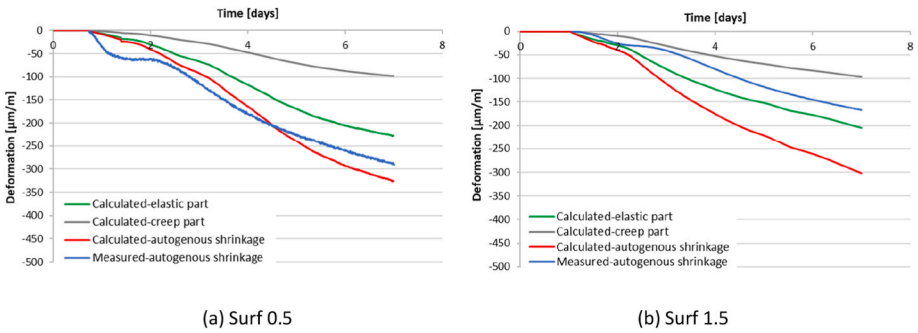

Fig. 19. Measured and calculated autogenous deformation of Portland cement paste with the addition of surfactant (0.5% and 1.5%) after maximum swelling.

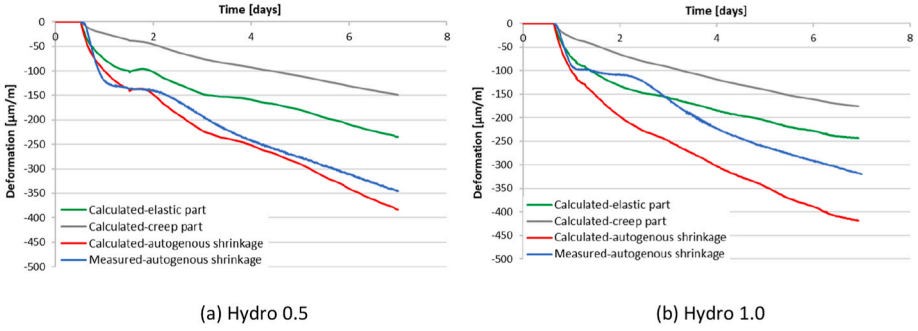

Fig. 20. Measured and calculated autogenous deformation of Portland cement paste with the addition of a water-repelling agent (0.5% and 1.0%) after maximum swelling.

However, when the dosage of the water-repelling agent increased from 0.5% to 1.0%, the measured results were almost the same (blue lines in Fig. 20a and b). As shown in Fig. 10, the contact angle between the capillary tube wall and the air-water interface of the mixtures with the addition of a water-repelling agent was larger than that of the reference. Therefore, the capillary tension of the mixtures with the addition of a water-repelling agent was lower than that of the reference, which led to a smaller autogenous shrinkage. However, when the dosage of the water-repelling agent was increased, the changes in the contact angle (Fig. 10e and f) and relative humidity (Fig. 11b) were negligible. The capillary tension of Hydro 0.5 and Hydro 1.0 is almost the same (Fig. 16). Meanwhile, the difference between the elastic modulus of Hydro 0.5 and Hydro 1.0 is also minimal. Therefore, the change in autogenous shrinkage with increasing dosage of the water-repelling agent was not remarkable. This indicates that there may be an optimum dosage of a water-repelling agent. Beyond the optimum dosage, the autogenous shrinkage did not decrease with the increasing dosage of the water-repelling agent. It should also be noted that although the autogenous shrinkages of Hydro 0.5 and Hydro 1.0 are similar, the strength of Hydro 1.0 is lower than that of Hydro 0.5 (Fig. 7). When the shrinkage of both mixtures is restrained, the risk of cracking of Hydro 1.0 should be higher than that of Hydro 0.5 due to its lower strength. This indicates that there should be an optimum dosage of the water-repelling agent. Beyond the optimum dosage, the effect of increasing the dosage of the water-repelling agent on the reduction in cracking risk is negative.

5.5. Discussion

Figs. 18–20 show the measured and calculated autogenous shrinkages of mixtures with and without admixtures. They show that the proposed model can be used to predict the autogenous shrinkage trend of mixtures with lower admixture dosages. However, there was a discrepancy between the measured and calculated autogenous shrinkage of the admixtures with higher dosages of surfactants and water-repelling agents.

In Fig. 19b, a significant difference between the measured and calculated autogenous shrinkages of the mixture with a 1.5% dosage of surfactant at 7 d was observed. The difference between the measured and calculated autogenous shrinkages may be attributed to the overestimated capillary tension. As explained in Section 5.3, the value of the calculated capillary tension is affected by the dissolved ions and the measured relative humidity (Equation (10)). The effect of dissolved ions in the pore solution on the calculated capillary tension changed with ion concentration. This study ignored the changes in the effect of dissolved ions. The ion concentration of pore water in cement paste increases with time during the first 28 d after mixing [109]. The influence of time on the calculated capillary tension also increases. The capillary tension was overestimated without considering the increasing ion concentration in pore water. The RH drop of Surf 1.5 is much smaller than that of the reference (Fig. 11b), and the influence of the ion concentration change on the calculated capillary tension and autogenous shrinkage was larger.

Fig. 20b shows that the autogenous shrinkage of cement paste with a 1.5% dosage of the water-repelling agent at seven days was overestimated using the proposed model. As discussed in Section 4.2, bleeding could be observed in mixtures with the addition of a water-repellent admixture during the first few hours after mixing [71]. A layer of water over the surface is reabsorbed into the cement paste at a later age. Reabsorbed water plays a role in internal curing, leading to smaller autogenous shrinkage [24]. With increasing dosage of the water-repelling agent, the bleeding and reabsorption phenomenon is more pronounced, and its effect on the mitigation is greater. In the proposed simulation model, the influence of bleeding and reabsorption on autogenous shrinkage is not considered, which may lead to a difference between the measured and calculated autogenous shrinkage of cement paste with a 1.5% dosage of a water-repelling agent.

In addition to ion concentration and bleeding, several other factors influencing autogenous deformation should be considered in this model to better predict autogenous shrinkage, such as early age expansion. Fig. 12 shows that the early age deformations observed at the

macroscale were the result of expansion and shrinkage processes that developed simultaneously. After the maximum swelling, the shrinkage process was dominant, and the external volume of the cement paste decreased. However, the expansion mechanism still plays a role in deformation, and neglecting its influence leads to an overestimation of the autogenous shrinkage. A quantitative simulation of the early age expansion will be beneficial in obtaining an accurate prediction of the autogenous deformation of cement paste.

In conclusion, to accurately predict the autogenous shrinkage of cement paste, some improvements, for example, by considering the change in ion concentration and early age swelling, are required in further research.

6. Conclusions

This study experimentally investigated the effects of surfactants and water-repelling agents on the material properties of Portland cement paste. According to the measurement results, the addition of a surfactant and water-repelling agent influenced the hydration process of the cement paste. Owing to the bleeding and reabsorption phenomena, the compressive strength of mixtures with the addition of a water-repellent admixture is lower than that of other mixtures with a similar degree of hydration. The surface tension of the pore solution decreased non-linearly with increasing surfactant dosage. The contact angle between the capillary tube wall and the air-pore solution interface increased with the addition of a water-repelling agent, but the effect of the water-repelling agent dosage on the change in the contact angle was not pronounced. The decrease in the relative humidity of both mixtures with the addition of the surfactant and water-repelling agent was smaller than that of the reference.

The material parameters, that is, the degree of hydration, degree of saturation, and capillary tension, were simulated based on the measurement results. The simulation results show that the addition of admixtures led to a lower degree of hydration and saturation. The capillary tension of the pure Portland cement was larger than that of the other mixtures. This can be attributed to several factors, including the smaller surface tension of mixtures with the surfactant, larger contact angle of mixtures with the water-repelling agent, and lower degree of hydration of mixtures with both admixtures. A simulation model that considered elastic deformation and creep was used to predict the autogenous shrinkage trend of different mixtures. Analyses of the simulated and measured results for different mixtures indicated that creep played an indispensable role in autogenous shrinkage. The addition of a surfactant and water-repelling agent can effectively mitigate autogenous shrinkage. However, when the dosage of the water-repelling agent was above a given value, its influence on the mitigation of autogenous shrinkage was insignificant. Therefore, there is an optimal dosage of water-repelling agents. Beyond the optimum dosage, the effect of increasing the dosage of the water-repelling agent on reducing the cracking risk can be negative. Based on a comparison between the simulated and measured results, the autogenous shrinkage trend can be predicted using the proposed model. However, improvements are required for the proposed model to accurately predict the magnitude of autogenous shrinkage.

CRediT authorship contribution statement

Tianshi Lu: conceptualisation, methodology, software, and writing of the original draft; Xuhui Liang: investigation; Chen Liu: investigation; Yun Chen: investigation; Zhenming Li: methodology, investigation, writing, review, and editing.

Declaration of competing interest

The authors declare that they have no known conflict of interest.

Data availability

Data will be made available on request.

Acknowledgment

The authors acknowledge the support of the China Scholarship Council (CSC), the Delft University of Technology (TU Delft), the National Natural Science Foundation of China (Grant Nos. 42271146) and Horizon Europe guarantee funding (grant number EP/X022587/1).

References

[1] K. Wang, D.C. Jansen, S.P. Shah, A.F. Karr, Permeability study of cracked concrete, Cement Concr. Res. 27 (3) (1997) 381–393.
[2] B. Gérard, J. Marchand, Influence of cracking on the diffusion properties of cement-based materials: Part I: influence of continuous cracks on the steady-state regime, Cement Concr. Res. 30 (1) (2000) 37–43.
[3] S.A. Altoubat, D.A. Lange, Creep, shrinkage, and cracking of restrained concrete at early age, ACI Mater. J. 98 (4) (2001) 323–331.
[4] P. Gao, Y. Chen, H. Huang, Z. Qian, E. Schlangen, J. Wei, Q. Yu, Investigation of drying-induced non-uniform deformation, stress, and micro-crack propagation in concrete, Cement Concr. Compos. 114 (2020), 103786.
[5] Y. Hu, Q. Li, R. Ma, Restrained cracking failure behavior of concrete due to temperature and shrinkage, Construct. Build. Mater. 244 (2020), 118318.
[6] M.S. Sule, K. Van Breugel, Effect of reinforcement on early-age cracking in high strength concrete, Heron 49 (3) (2004).
[7] B.F. Dela, L.F. Nielsen, H. Stang, Determination of eigenstresses in hardening concrete, in: 16th Symposium on Nordic Concrete Research, Norsk Betongforening, 1996, pp. 25–26.
[8] E.E. Holt, Early Age Autogenous Shrinkage of Concrete, University of Washington, 2001.
[9] M. Geiker, T. Knudsen, Chemical shrinkage of Portland cement pastes, Cement Concr. Res. 12 (5) (1982) 603–610.
[10] E.I. Tazawa, S. Miyazawa, T. Kasai, Chemical shrinkage and autogenous shrinkage of hydrating cement paste, Cement Concr. Res. 25 (2) (1995) 288–292.
[11] T.C. Powers, A Hypothesis on Carbonation Shrinkage (No. 146), 1962.
[12] Y.F. Houst, Carbonation shrinkage of hydrated cement paste, in: Proc. 4th CANMET/ACI International Conference on Durability of Concrete (No. CONF, CANMET, Ottawa, Canada, 1997, pp. 481–491.
[13] P. Lura, Autogenous Deformation and Internal Curing of Concrete, Technische Universiteit Delft, 2003. Doctoral dissertation, Ph. D. Thesis.
[14] Y. Wei, Modeling of Autogenous Deformation in Cementitious Materials, Restraining Effect from Aggregate, and Moisture Warping in Slabs on Grade, University of Michigan, 2008. Doctoral dissertation, Ph. D. Thesis.
[15] Z. Hu, M. Wyrzykowski, K. Scrivener, P. Lura, Prediction of autogenous shrinkage of cement pastes as poro-visco-elastic deformation, Cement Concr. Res. 126 (2019), 105917.
[16] T. Lu, Autogenous Deformation of Early Age Cement Paste and Mortar, Technische Universiteit Delft, 2019. Doctoral dissertation, Ph. D. Thesis.
[17] Z. Li, Autogenous Shrinkage of Alkali-Activated Slag and Fly Ash Materials from Mechanism to Mitigating Strategies, Technische Universiteit Delft, 2021. Doctoral dissertation, Ph. D. Thesis.
[18] Zhenming Li, et al., Chemical deformation of metakaolin based geopolymer, Cement Concr. Res. 120 (2019) 108–118.
[19] E.I. Tazawa, Autogenous Shrinkage of Concrete, CRC Press, 1999.
[20] Zhenming Li, et al., Mechanisms of autogenous shrinkage of alkali-activated slag and fly ash pastes, Cement Concr. Res. 135 (2020) 106107.
[21] A. Bentur, S.I. Igarashi, K. Kovler, Prevention of autogenous shrinkage in high-strength concrete by internal curing using wet lightweight aggregates, Cement Concr. Res. 31 (11) (2001) 1587–1591.
[22] D.P. Bentz, O.M. Jensen, Mitigation strategies for autogenous shrinkage cracking, Cement Concr. Compos. 26 (6) (2004) 677–685.
[23] E.I. Tazawa, S. Miyazawa, Experimental study on mechanism of autogenous shrinkage of concrete, Cement Concr. Res. 25 (8) (1995) 1633–1638.
[24] M.R. Geiker, D.P. Bentz, O.M. Jensen, Mitigating Autogenous Shrinkage by Internal Curing, ACI Special Publications, 2004, pp. 143–154.
[25] G. Pickett, Effect of aggregate on shrinkage of concrete and a hypothesis concerning shrinkage, Journal Proceedings 52 (1) (1956, January) 581–590.
[26] P.K. Mehta, Mechanism of expansion associated with ettringite formation, Cement Concr. Res. 3 (1) (1973) 1–6.
[27] P.M. Zhan, Z.H. He, Application of shrinkage reducing admixture in concrete: a review, Construct. Build. Mater. 201 (2019) 676–690.
[28] M.J. Rosen, J.T. Kunjappu, Surfactants and Interfacial Phenomena, John Wiley & Sons, 2012.
[29] R. Gagné, Shrinkage-reducing admixtures, in: Science and Technology of Concrete Admixtures, Woodhead Publishing, 2016, pp. 457–469.
[30] D.R. Karsa, P.J. Donnelly, J.M. Goode, Surfactants Applications Directory, Springer Science & Business Media, 2012.
[31] Z. Qu, Design and Performance of Water Resistant Cementitious Materials, Technische Universiteit Eindhoven, 2020. Doctoral dissertation, Ph. D. Thesis.

[32] H.S. Wong, R. Barakat, A. Alhilali, M. Saleh, C.R. Cheeseman, Hydrophobic concrete using waste paper sludge ash, Cement Concr. Res. 70 (2015) 9–20.
[33] Z.Y. Qu, F. Gauvin, F.Z. Wang, G. Liu, H.J.H. Brouwers, Effect of hydrophobicity on autogenous shrinkage and carbonation of alkali activated slag, Construct. Build. Mater. 264 (2020), 120665.
[34] M. Collepardi, A. Borsoi, S. Collepardi, J.J.O. Olagot, R. Troli, Effects of shrinkage reducing admixture in shrinkage compensating concrete under non-wet curing conditions, Cement Concr. Compos. 27 (6) (2005) 704–708.
[35] S. Anshuang, Q. Ling, Z. Shoujie, Z. Jiayang, L. Zhaoyu, Effects of shrinkage reducing agent and expansive admixture on the volume deformation of ultrahigh performance concrete, Adv. Mater. Sci. Eng. 2017 (2017).
[36] J. Feij, Shrinkage Reducing Agent in Concrete: the Mechanism and its Influences on the Hydration Process and Mechanical Properties, Technische Universiteit Delft, 2020. Master Thesis.
[37] J. Carette, B. Delsaute, N. Milenković, J.P. Lecomte, M.P. Delplancke, S. Staquet, Advanced characterisation of the early age behaviour of bulk hydrophobic mortars, Construct. Build. Mater. 267 (2021), 120904.
[38] A.M. Neville, Creep of Concrete: Plain, Reinforced, and Prestressed, 1971.
[39] Z.P. Bazant, F.H. Wittmann, Creep and Shrinkage in Concrete Structures, 1982.
[40] A.D. Ross, Creep of concrete under variable stress, Journal Proceedings 54 (3) (1958, March) 739–758.
[41] Z.P. Bazant, S. Prasannan, Solidification theory for aging creep, Cement Concr. Res. 18 (6) (1988) 923–932.
[42] B. Hedegaard, Creep and shrinkage modeling of concrete using solidification theory, J. Mater. Civ. Eng. 32 (7) (2020), 04020179.
[43] P. Lura, O.M. Jensen, K. Van Breugel, Autogenous shrinkage in high-performance cement paste: an evaluation of basic mechanisms, Cement Concr. Res. 33 (2) (2003) 223–232.
[44] Z. Hu, Prediction of Autogenous Shrinkage in Fly Ash Blended Cement Systems (No. THESIS), EPFL, 2017.
[45] C. Hua, P. Acker, A. Ehrlacher, Analyses and models of the autogenous shrinkage of hardening cement paste: I. Modelling at macroscopic scale, Cement Concr. Res. 25 (7) (1995) 1457–1468.
[46] M.J. Setzer, „The munich model-an example for modern materials science in. Civil engineering, in: A. Gerdes (Ed.), Advances in Building Materials Science-Research and Applications, AEDIFICATIO Publishers, Freiburg and Unterengstringen, 1996, p. 3.
[47] L.F. Nielsen, A Research Note on Sorption, Pore Size Distribution, and Shrinkage of Porous Materials. Danmarks Tekniske Højskole. Laboratoriet for Bygningsmaterialer, 1991.
[48] K. Kovler, S. Zhutovsky, Overview and future trends of shrinkage research, Mater. Struct. 39 (9) (2006) 827–847.
[49] R. Defay, I. Prigogine, A. Bellemans, Surface Tension and Adsorption, Wiley, 1966.
[50] K. Van Breugel, Simulation of Hydration and Formation of Structure in Hardening Cement-Based Materials, Technische Universiteit Delft, 1993. Doctoral dissertation, Ph. D. Thesis.
[51] W.G. Gray, B.A. Schrefler, Thermodynamic approach to effective stress in partially saturated porous media, Eur. J. Mech. Solid. 20 (4) (2001) 521–538.
[52] M.M. Alam, M.K. Borre, I.L. Fabricius, K. Hedegaard, B. Røgen, Z. Hossain, A. S. Krogsbøll, Biot's coefficient as an indicator of strength and porosity reduction: calcareous sediments from Kerguelen Plateau, J. Petrol. Sci. Eng. 70 (3–4) (2010) 282–297.
[53] D. Gawin, F. Pesavento, B.A. Schrefler, Modelling creep and shrinkage of concrete by means of effective stresses, Mater. Struct. 40 (6) (2007) 579–591.
[54] X. Wang, S. Yuan, B. Jiang, Wetting process and adsorption mechanism of surfactant solutions on coal dust surface, J. Chem. 2019 (2019).
[55] W.L. Hinze, H.N. Singh, Y. Baba, N.G. Harvey, Micellar enhanced analytical fluorimetry, TrAC, Trends Anal. Chem. 3 (8) (1984) 193–199.
[56] J. De Vries, R.B. Polder, Hydrophobic treatment of concrete, Construct. Build. Mater. 11 (4) (1997) 259–265.
[57] R. Di Mundo, C. Labianca, G. Carbone, M. Notarnicola, Recent advances in hydrophobic and icephobic surface treatments of concrete, Coatings 10 (5) (2020) 449.
[58] C. Astm, Standard practice for mechanical mixing of hydraulic cement pastes and mortars of plastic consistency, Am. Soc. Test. Mater. (1999) 305–399.
[59] EN, B. 196–8, Methods of Testing Cement. Heat of Hydration. Solution Method, 2010.
[60] D. En, Methods of Testing Cement—Part 3: Determination of Setting Times and Soundness, 2009.
[61] M. Azenha, F. Magalhães, R. Faria, Á. Cunha, Measurement of concrete E-modulus evolution since casting: a novel method based on ambient vibration, Cement Concr. Res. 40 (7) (2010) 1096–1105.
[62] O. Büyüköztürk, M.A. Taşdemir, in: Nondestructive Testing of Materials and Structures, vol. 6, Springer Science & Business Media, 2012.
[63] ASTM International, Standard Test Method for Surface and Interfacial Tension of Solutions of Paints, Solvents, Solutions of Surface-Active Agents, and Related Materials, 2014. D1331-14.
[64] B. Feneuil, O. Pitois, N. Roussel, Effect of surfactants on the yield stress of cement paste, Cement Concr. Res. 100 (2017) 32–39.
[65] ASTM International, Standard Test Method for Autogenous Strain of Cement Paste and Mortar, 2009. C1698-09.
[66] K. Van Breugel, Numerical simulation of hydration and microstructural development in hardening cement-based materials, Heron 37 (3) (1992).
[67] S. Mindess, F.J. Young, D. Darwin, Concrete, second ed., Technical Documents, 2003.
[68] W. Zuo, P. Feng, P. Zhong, Q. Tian, N. Gao, Y. Wang, C. Yu, C. Miao, Effects of novel polymer-type shrinkage-reducing admixture on early age autogenous deformation of cement pastes, Cement Concr. Res. 100 (2017) 413–422.
[69] ASTM, ASTM C125-Standard Terminology Relating to Concrete and Concrete Aggregates, 2018.
[70] B.H. Ahmadi, Initial and final setting time of concrete in hot weather, Mater. Struct. 33 (8) (2000) 511–514.
[71] Z. Lu, X. Zhou, J. Zhang, Study on the performance of a new type of water-repellent admixture for cement mortar, Cement Concr. Res. 34 (11) (2004) 2015–2019.
[72] G. Giaccio, A. Giovambattista, Bleeding: evaluation of its effects on concrete behaviour, Mater. Struct. 19 (4) (1986) 265–271.
[73] P. Liu, C. Feng, F. Wang, Y. Gao, J. Yang, W. Zhang, L. Yang, Hydrophobic and water-resisting behavior of Portland cement incorporated by oleic acid modified fly ash, Mater. Struct. 51 (2) (2018) 1–9.
[74] R. Shahbazi, A.H. Korayem, A. Razmjou, W.H. Duan, C.M. Wang, H. Justnes, Integrally hydrophobic cementitious composites made with waste amorphous carbon powder, Construct. Build. Mater. 233 (2020), 117238.
[75] B. Henk, THE EARLY STRENGTH OF CONCRETE UNDER NATURAL CONDITIONS OF HARDENING, Betonstein-zeitung, Weisbaden/Germany, 1966.
[76] V.K. Kumar, A.K. Priya, G. Manikandan, A.S. Naveen, B. Nitishkumar, P. Pradeep, Review of materials used in light weight concrete, Mater. Today: Proc. 37 (2021) 3538–3539.
[77] M.F.M. Zain, M. Safiuddin, I.A.A.A. Mohamed, Influence of different curing methods on the compressive strength and modulus of elasticity of high performance concrete, in: Proceedings of the Sixth International Conference on Concrete Engineering and Technology, 1999, June, pp. 13–25. Kuala Lumpur, Malaysia.
[78] B.D. Liu, W.J. Lv, L. Li, P.F. Li, Effect of moisture content on static compressive elasticity modulus of concrete, Construct. Build. Mater. 69 (2014) 133–142.
[79] Zhenming Li, et al., Prediction of the autogenous shrinkage and microcracking of alkali-activated slag and fly ash concrete, Cement Concr. Compos. 117 (2021) 103913.
[80] N.B. Vargaftik, B.N. Volkov, L.D. Voljak, International tables of the surface tension of water, J. Phys. Chem. Ref. Data 12 (3) (1983) 817–820.
[81] M. Jensen, P.F. Hansen, Autog enous deformation and change of the relative humidity in silica fume-modified cement paste, Mater. J. 93 (6) (1996) 539–543.
[82] P, O.M. Jensen, K.K. Hansen, J.F. Olesen, H. Stang, C.J. Haecker, Influence of cement particle-size distribution on early age autogenous strains and stresses in cement-based materials, J. Am. Ceram. Soc. 84 (1) (2001) 129–135.
[83] P. Perrot, A to Z of Thermodynamics, Oxford University Press on Demand, 1998.
[84] D.P. Bentz, M.R. Geiker, K.K. Hansen, Shrinkage-reducing admixtures and early-age desiccation in cement pastes and mortars, Cement Concr. Res. 31 (7) (2001) 1075–1085.
[85] P. Lura, O.M. Jensen, K. Van Breugel, Autogenous shrinkage in high-performance cement paste: an evaluation of basic mechanisms, Cement Concr. Res. 33 (2) (2003) 223–232.
[86] E.M. Winkler, P.C. Singer, Crystallization pressure of salts in stone and concrete, Geol. Soc. Am. Bull. 83 (11) (1972) 3509–3514.
[87] Y. Tezuka, J.G. Djanikan, H. Uchikawa, S. Uchida, Hydration characteristics and properties of mixtures of cement and high content of calcium, in: Proc. Symp. On Chemistry of Cement, 1986, pp. 323–329. Rio de Janeiro, Bresil.
[88] B. Delsaute, S. Staquet, Monitoring of the thermal and autogenous strain, in: Advanced Techniques for Testing of Cement-Based Materials, Springer, Cham, 2020, pp. 135–176.
[89] M. Chang-Wen, T. Qian, S. Wei, L. Jia-Ping, Water consumption of the early-age paste and the determination of "time-zero" of self-desiccation shrinkage, Cement Concr. Res. 37 (11) (2007) 1496–1501.
[90] J. Weiss, 6.1 experimental determination of the 'time-Zero'tO (Maturity-Zero MO), in: Report 25: Early Age Cracking in Cementitious Systems-Report of RILEM Technical committee TC 181-EAS: Early age cracking shrinkage induced stresses and cracking in cementitious systems, 25, 2003, p. 195.
[91] Ø. Bjøntegaard, Thermal Dilatation and Autogenous Deformation as Driving Forces to Self-Induced Stresses in High Performance Concrete, Norwegian University of Science and Technology, Norway, 1999. Ph.D. Thesis.
[92] L.J. Parrott, M. Geiker, W.A. Gutteridge, D. Killoh, Monitoring Portland cement hydration: comparison of methods, Cement Concr. Res. 20 (6) (1990) 919–926.
[93] W. Lerch, Uber die Hydratationswarme des Portlandzements, Zement-Kalc-Gips 14 (11) (1935) 155–158.
[94] G. Ye, Experimental Study and Numerical Simulation of the Development of the Microstructure and Permeability of Cementitious Materials, Technische Universiteit Delft, 2003. Doctoral dissertation, Ph. D. Thesis.
[95] T.C. Powers, T.L. Brownyard, Studies of the physical properties of hardened Portland cement paste, Journal Proceedings 43 (9) (1946, September) 101–132.
[96] O.M. Jensen, Autogenous Deformation and RH-Change – Self-Desiccation and Self-Desiccation Shrinkage. Appendix - Measurements and Notes, Building Materials Laboratory, The Technical University of Denmark, Lyngby, Denmark, 1993 (in Danish), TR 285/93.
[97] O.M. Jensen, P.F. Hansen, Water-entrained cement-based materials: I. Principles and theoretical background, Cement Concr. Res. 31 (4) (2001) 647–654.
[98] L. Struble, P. Hawkins, P. Klieger, J.F. Lamond, Hydraulic Cements-Physical Properties: Significance of Tests and Properties of Concrete and Concrete-Making Materials", ASTM International, West Conshohocken PA, 1994.
[99] B. Lebental, W. Moujahid, C.S. Lee, J.L. Maurice, C.S. Cojocaru, Graphene-based resistive humidity sensor for in-situ monitoring of drying shrinkage and intrinsic

permeability in concrete, in: NICOM 4: 4th International Symposium on Nanotechnology in Construction, 2012, May, p. 8p.
[100] P. Acker, F.J. Ulm, Creep and shrinkage of concrete: physical origins and practical measurements, Nucl. Eng. Des. 203 (2–3) (2001) 143–158.
[101] P. Klug, F. Wittmann, Activation energy of creep of hardened cement paste, Matériaux et Construction 2 (1) (1969) 11–16.
[102] Z.P. Bažant, J.C. Chern, Double-power logarithmic law for concrete creep, Cement Concr. Res. 14 (6) (1984) 793–806.
[103] Z.P. Bazant, J.C. Chern, Log double power law for concrete creep, ACI J. Proc. 82 (5) (1985, September) 665–675.
[104] P. Gao, G. Ye, H. Huang, Z. Qian, E. Schlangen, J. Wei, Q. Yu, Incorporating elastic and creep deformations in modelling the three-dimensional autogenous shrinkage of cement paste, Cement Concr. Res. 160 (2022), 106907.
[105] Z. Bažant, M. Hubler, R. Wendner, Model B4 for Creep, Drying Shrinkage and Autogenous Shrinkage of Normal and High-Strength Concretes with Multi-Decade Applicability, RILEM Technical Committee TC-242-MDC, 2015, p. 9.
[106] G.C. Fanourakis, Validation of the FIB 2010 and RILEM B4 models for predicting creep in concrete, Archit. Civil Eng. Environ. 95 (2017) 95–101.
[107] Z.P. Bazant, S. Prasannan, Solidification theory for concrete creep. I: formulation, J. Eng. Mech. 115 (8) (1989) 1691–1703.
[108] Z.P. Bažant, S. Prasannan, Solidification theory for concrete creep. II: verification and application, J. Eng. Mech. 115 (8) (1989) 1704–1725.
[109] H.F. Taylor, in: Cement Chemistry, vol. 2, Thomas Telford, London, 1997, p. 459.